OPEN ACCESS
IOP Publishing
Plasma Physics and Controlled Fusion
Plasma Phys. Control. Fusion **65** (2023) 034007 (8pp)
https://doi.org/10.1088/1361-6587/acb080

Creating pair plasmas with observable collective effects

Kenan Qu[1,*], **Sebastian Meuren**[2] **and Nathaniel J Fisch**[1]

[1] Department of Astrophysical Sciences, Princeton University, Princeton, NJ 08544, United States of America
[2] Stanford PULSE Institute, SLAC National Accelerator Laboratory, Menlo Park, CA 94025, United States of America

E-mail: kq@princeton.edu

Received 30 September 2022, revised 6 December 2022
Accepted for publication 5 January 2023
Published 15 February 2023

Abstract

Although existing technology cannot yet directly produce fields at the Schwinger level, experimental facilities can already explore strong-field quantum electrodynamics (QED) phenomena by taking advantage of the Lorentz boost of energetic electron beams. Recent studies show that QED cascades can create electron–positron pairs at sufficiently high density to exhibit collective plasma effects. Signatures of collective pair plasma effects can appear in exquisite detail through plasma-induced frequency upshifts and chirps in the laser spectrum. Maximizing the magnitude of the QED plasma signature demands high pair density and low pair energy, which suits the configuration of colliding an over 10^{18} J m^{-3} energy-density electron beam with a 10^{22}–10^{23} W cm^{-2} intensity laser pulse. The collision creates pairs that have a large plasma frequency, made even larger as they slow down or reverse direction due to both the radiation reaction and laser pressure. This paper explains at a tutorial level the key properties of the QED cascades and laser frequency upshift, and at the same time finds the minimum parameters that can be used to produce observable QED plasma.

Keywords: quantum electrodynamics, electron–positron pairs, ultra-intense laser, plasmas, laser frequency upshift

(Some figures may appear in colour only in the online journal)

1. Introduction

According to quantum electrodynamics (QED) theory, when the field exceeds the Schwinger limit [1] $E_{\rm cr}$, the quantum vacuum becomes unstable and it spontaneously creates pairs of electrons and positrons. The oppositely charged electrons and positrons at high density naturally lead to collective plasma effects in the so-called 'QED plasma' regime [2–7]. QED plasma effects dominate in astrophysical environments such as near a black hole [8] or magnetar [9, 10]. Our current understanding of these environments [11] is based upon strong-field QED theory for pair creation and plasma theory for the subsequent pair–pair interactions. However, to accurately describe how the QED pair plasmas emit observable radiation and affect the information delivery in the cosmological horizon, it is critical to address the interplay of collective plasma and strong-field QED processes.

Recent progress in the study of QED physics has been stimulated by the advances of high-power laser technology. Since the invention of chirped-pulse amplification [12–14], the record laser intensity [15] has grown steadily from 10^{15} to 10^{23} W cm^{-2}. Although the latter number is still six orders of magnitude lower than needed for providing $E_{\rm cr}$, we can bridge the gap by colliding the laser with an energetic electron beam. Ultra-relativistic electrons boost the laser field by

* Author to whom any correspondence should be addressed.

Original Content from this work may be used under the terms of the Creative Commons Attribution 4.0 licence. Any further distribution of this work must maintain attribution to the author(s) and the title of the work, journal citation and DOI.

 © 2023 The Author(s). Published by IOP Publishing Ltd

orders of magnitude in the electron rest frame, making it possible for existing lasers to test quantum effects. Applying this method, the seminal Stanford E-144 experiment [16, 17] in the 1990s detected evidence of positron creation using a 10^{18} W cm^{-2} laser colliding with a near 50 GeV electron beam. The quantum nonlinearity parameter, defined as the ratio of the field to the critical field, is $\chi = E^*/E_{\rm cr} \sim 0.3$ (E^* is measured in the electron rest frame) for this experiment. Two decades later, the Gemini laser facility [18, 19] employed a 4×10^{20} W cm^{-2} laser pulse colliding with a GeV electron beam, created via laser wakefield acceleration (LWFA), to observe signatures of quantum radiation reaction at $\chi \sim 0.1$. The commissioned E-320 experiment [20] is designed to extend the Stanford experiment and collide a 10^{20} W cm^{-2} laser with 10 GeV electron beam to reach $\chi \sim 1$.

While the community is focusing on testing QED effects at the single particle level, we note that the technology for accessing the QED plasma regime is, in fact, already available [6, 7]. Suppose we can colocate a 10^{23} W cm^{-2} laser with the 30 GeV electron beam at SLAC [21, 22]; then, the χ parameter reaches $\sim$100 which is sufficient to produce a QED cascade [23–34]. Such a cascade, shown in recent numerical simulations [6, 7], creates pairs at sufficiently high density and low energy that the collective plasma effects begin to show signatures during the laser-pair interaction.

However, creating a QED plasma and probing its collective effects, while technically possible, is not so simple. First, the created pairs gain high energy either directly from the gamma photons, which they decay from or from the strong laser field. The high pair energy represents an increased relativistic mass, which significantly suppresses their contribution to collective plasma effects. Second, even with extreme parameters, such as a 10^{23} W cm^{-2} laser and a 1 nC, 30 GeV electron beam, the created pair plasma only has a charge of $\sim$100 nC distributed in micron scale. The low charge number and small volume prohibit the onset of most plasma instabilities. Third, the pair particles are subject to the ponderomotive force of the intense laser, and they undergo rapid volume expansion. Already traveling at relativistic speeds, pair particles last as a plasma within the laser for only picoseconds, as numerically demonstrated in [6, 7].

Thus, detecting subtle collective effects in QED plasma requires methods that are sensitive and robust. In view of the aforementioned challenges, we suggest [6, 7] employing a 10^{23} W cm^{-2} laser to collide with a *dense* high energy electron beam. The induced QED cascade can not only produce pairs at high density but also at low energy. Both properties contribute to strong collective plasma effects. More importantly, the laser pulse, while creating the QED cascade, also probes the time varying pair plasma through the induced frequency change [35–47]. The laser frequency upshift, determined solely by the change of plasma frequency, provides a robust and unambiguous signature of the collective plasma effects.

In this paper, we elaborate on the joint production-observation problem of collective effects in QED plasmas. We analyze the available technologies and assess their advantages for producing high-density and low-energy pair plasmas. In section 2, we compare the laser-laser collision approach and the beam-laser collision approach for creating plasma and for reducing the relativistic boost of the pair mass. In section 3, we find the conditions on the energy density of the electron beam that can create an observable pair plasma. To provide the electron beam, we demonstrate the availability of existing conventional electron beam facilities and the promise of the LWFA method at high-power laser facilities. In section 4, we explain in detail how the laser frequency spectrum changes in a time-varying plasma and derive the amount of laser frequency upshift. In section 5, we present our conclusion.

2. Reducing the pair energy for strong plasma signatures

The plasma frequency is determined by both the pair density n_p and the pair energy (proportional to its Lorentz factor γ): $\omega_p = \sqrt{n_p e^2/(\epsilon_0^2 \gamma m_e)}$, where e is the natural charge, ε_0 is the vacuum permittivity, and m_e is the pair rest mass. It is thus key to prepare QED pairs at low energy for detecting their collective effects. Otherwise, high particle energy causes large pair mass from relativistic effects and would substantially suppress their collective response. The requirement of low pair energy seems to conflict with the QED condition that gamma photon emission takes place only with high energy particles. This is true with the laser-laser collision approach for reaching the QED regime, but the conflict is avoided in an electron-beam driven QED cascade.

2.1. Laser-laser collision cascade

A laser-laser collision approach of QED cascade, also referred to as the 'avalanche-type' cascade, employs two ultra-intense counterpropagating laser pulses overlapping in a region with stationary seed electrons [48, 49]. The strong laser beat wave accelerates the electrons to relativistic velocities. As the electron Lorentz factor γ increases, the laser field is boosted by an increasing factor to reach the quantum critical field. Once the quantum nonlinearity parameter $\chi = \gamma E/E_{\rm cr}$ reaches near unit value, the electrons begin to emit high energy gamma photons that can decay into electron–positron pairs. The pairs are then accelerated by the laser field to continue the QED process and develop into a cascade. This process is 'self-sustained', i.e. it terminates only when the pairs escape the laser focal region.

In order to reach the QED cascade condition, the laser-laser collision approach [3, 49] likely requires 10^{24} W cm^{-2} laser intensities, corresponding to laser amplitude $a_0 \equiv eE/(m_e c^2 \omega_0) \sim 10^3$, where ω_0 is the laser frequency. If a pair plasma is created, the pair particles would be quickly accelerated to high energy with Lorentz factors $\gamma > 10^3$. Thus, their contribution to the plasma frequency could be suppressed by a factor of at least 10^3. The smallness of their contribution means that detecting collective plasma effects would require higher pair density, which in turn requires even stronger lasers. Moreover, because of the high pair energy, the contribution of the pairs to the collective plasma effects can be less than that

of the stationary seeding electrons unless the pair number multiplication factor is larger than $\gamma > a_0 \sim 10^3$.

2.2. Electron-beam driven cascade

In contrast to the laser-laser collision approach, the electrons in a beam-driven QED cascade begin with the maximum particle energy. Once the ramping-up laser intensity reaches $\chi = 2\gamma E/E_{\rm cr} \geqslant 1$ in the boosted frame (the factor of 2 arises from the counterpropagating configuration), the electrons begin to emit gamma photons and lose significant energy. Electron–positron pairs are created by acquiring the energy of the emitted gamma photons. If the pairs have sufficiently high Lorentz factors, i.e. $\chi \geqslant 1$, they emit more gamma photons that can decay into more pairs. This process is thus also called the 'shower-type' QED cascade. This type of cascade converts electron beam energy into pair particles during its collision with a strong laser. However, the laser pulse does not contribute to the pair energy. The created pairs exhibit increasingly strong plasma behavior both when their density grows and when their energy decreases. This approach takes advantage of the high beam energy available through existing electron beam facilities; hence, it greatly reduces the required laser intensity. For example, with 30 GeV electron beam energy, 10^{20} W cm^{-2} laser intensity can already reach $\chi \geqslant 1$ and produce pair number multiplication. A higher laser intensity at 10^{22}–10^{23} W cm^{-2}, combined with the same electron beam, could reach the extreme quantum limit $\chi \gg 1$ and induce a fully-featured QED cascade [6, 7].

The low requirement for laser intensity not only avoids the technical challenges of building 100 PW-class laser, but also allows the pairs to exhibit strong plasma effects. In the electron-beam driven cascade, the counterpropagating laser pulse decelerates the particles to reduce the pair energy. This means that the relativistic particle mass decreases and their contribution to the plasma frequency increases. The minimum pair energy (and hence the maximum contribution to the plasma frequency) is achieved if the pairs could be fully stopped, at least, in the longitudinal direction. In the 'pair-stopping' regime, the minimum pair energy is then determined solely by their transverse quiver motion driven by the laser, and thus $\gamma \sim a_0$ for $a_0 \gg 1$.

Reaching the 'pair-stopping' regime requires the laser amplitude to exceed a threshold value: $a_{0,\rm th} \approx 100$ corresponding to $I_{0,\rm th} \approx 10^{22}$–$10^{23}$ W cm^{-2} for μm-wavelength lasers. The threshold laser amplitude is obtained [6, 7] by analyzing the two dominating mechanisms of pair deceleration. The high energy pairs first lose energy mainly through the quantum radiation reaction, which terminates when the pair energy decreases below the value for $\chi(\propto a_0\gamma) \lesssim 0.1$. Then, the second mechanism—the ponderomotive force of the counterpropagating laser—begins to dominate the pair deceleration. The ponderomotive pressure can reduce the longitudinal electron momentum by the maximum amount of $\gamma m_e c \cong a_0 m_e c$ in the limit of a single laser wavelength [23], and this value is slightly larger for longer laser pulses [50]. These two mechanisms scale with a_0 differently. By equating the terminal pair energy for quantum radiation reaction and the maximum pair energy that can be exchanged with the laser field, we can find the threshold laser amplitude: $a_{0,\rm th} \approx 100$. Above this threshold, the pair particles could be fully stopped reaching the minimum longitudinal momentum.

If the laser intensity substantially exceeds $I_{0,\rm th}$, some of the pair particles, if they remain near the laser center, could be reaccelerated by a strong ponderomotive force toward the laser beam direction. The reacceleration, on one hand, increases the pair Lorentz factor, but, on the other hand, also reduces the laser frequency in the pair rest frame. For the particular plasma signature of laser frequency upshift, it is shown [50] that reacceleration can accentuate the amount of frequency upshift by up to a factor of 2.

3. Reaching high pair density for large plasma effects

In an electron-beam driven QED cascade, all the pairs are created by converting the energy of either the electron beam or the pairs created by it, mediated by high energy gamma photons. Since the energy contribution from the laser and long-wavelength emissions are both negligible, the total particle energy is conserved during the cascade. In other words, the integrated particle energy-density over the whole space is conserved.

The conservation of integrated particle energy-density means that creating a high density pair plasma requires employing a high energy-density electron beam. Quantitatively, the final pair density n_p can be estimated as

$$n_p \approx n_0 \chi_0, \tag{1}$$

where n_0 is the density of injected electrons and $\chi_0 \approx 2a_0\gamma_0(\hbar\omega_0)/(m_e c^2)$, interpreted as the pair multiplication factor, is the quantum nonlinearity parameter for the injected electron beam with γ_0 in the laser field. This relation assumes that all the pair particles interact with constant laser intensity and the cascade terminates at $\chi \sim 1$ when their emitted photons can no longer decay into more pairs. For μm-wavelength lasers, the relation can be written numerically as $n_p \approx 4 \times 10^{-6} a_0\gamma_0 n_0$. Thus, for the cascade to create a pair density near the critical density $n_p \sim 2 \times 10^{21}$ cm^{-3}, the electron beam needs to have energy density $\gamma_0 n_0 \sim 10^{25}$ cm^{-3} assuming that the laser reaches at the 'pair-stopping' threshold amplitude ($a_0 \approx 100$).

Note that, although employing a higher laser intensity can improve the pair multiplication factor, it does not always increase the pair plasma frequency. Once the laser amplitude is above $a_{0,\rm th}$, the final pair motion becomes dominantly transverse with kinetic energy proportional to the laser amplitude. Higher laser amplitude simultaneously induces a larger pair multiplication factor and a larger Lorentz factor, canceling their contribution to the plasma frequency $\omega_p \propto \sqrt{n_p/\gamma}$.

The required high energy-density $\gamma_0 n_0 \sim 10^{25}$ cm^{-3} naturally favors conventional accelerators due to their high luminosity. For GeV-level electron beam, the density needs to reach 10^{19} cm^{-3}. For example, the nC-level electron charge is accessible in several electron accelerator facilities including

SLAC, eRHIC, ILC, CLIC, etc. Taking into account the beam bunch size, their electron densities all exceed 10^{19} cm^{-3}. Notably, their beam energy is in the range of 10 GeV to TeV level enabling $\gamma_0 n_0 \sim 10^{27}$–$10^{30}$ cm^{-3}.

LWFA is an alternative technique, which yields hundreds-of-MeV GeV-level electron beams at high-power laser facilities. It uses the ponderomotive force of a strong laser pulse to push plasma electrons via either a self-modulated beat wave or a hollow bubble. Current LWFA techniques, however, have the major drawback of a trade-off between high beam energy and high charge number. The current record [51] for LWFA electron energy is ∼8 GeV, but it only has ∼5 pC total charge. The energy density of this electron beam is still three orders of magnitude lower than the required value. Higher charge number could be achieved only by compromising the beam length and more importantly the beam energy, which both reduce the energy density. Recent studies [52–55] show via numerical simulation that long-wavelength CO_2 lasers at high power might overcome the energy-density barrier and produce high electron charge numbers at the GeV level through LWFA. Nevertheless, producing 1 nC of electrons at 10 GeV, which contains 10 J electron kinetic energy, will need next generation laser technology capable of delivering 100–1000 J laser pulses even at 1%–10% energy conversion efficiency.

4. Laser frequency upshift induced by plasma effects

If a pair plasma was created through the QED cascade as we described above, it would be micrometer sized with relativistic velocity making diagnosing it challenging. Detecting subtle collective effects requires unconventional methods that are sensitive and robust. One of the lowest order plasma effects is the dispersion relation. As the pair plasma is formed, the plasma frequency grows both when the pair density increases and when the pair energy decreases. The growing plasma frequency changes the dispersion relation of the laser by reducing the refractive index and increasing the laser phase velocity. Sudden creation of plasma over space amounts to a temporal interface of refractive indices, through which the laser frequency is upshifted. Considering that the pair plasma dimension is only a fraction of the laser duration, the increased laser phase velocity also causes its wavefront to compress toward the front, which can be detected as a chirp in the laser spectrum. Both the laser frequency upshift and chirp arise from the temporal evolution of the plasma frequency, hence they serve as unambiguous signatures of collective effects.

The creation of a pair plasma is modeled as a temporal interface of refractive indices, which is known to cause laser frequency upshift [40, 56–59]. The frequency upshift process [36–38, 41–47] is analogous to the trivial process of laser wavelength shift when crossing a spatial interface of refractive indices. The concept of laser frequency change in dynamic media was first studied [35] theoretically by Morgenthaler in 1958. With the rapidly growing laser technology in the 1970s, it is found [60–62] that laser-breakdown plasmas can serve as such dynamic media. The concept was further developed as, so-called, 'photon accelerators' [39, 63–66], in which the laser propagates in the rear edge of a plasma wave wakefield. Since the laser co-moves in a positive density gradient, it can be frequency upconverted continuously. Using laser-induced ionization, frequency upconversion has been experimentally demonstrated in the microwave [66–70], terahertz [43] and optical [71, 72] regimes.

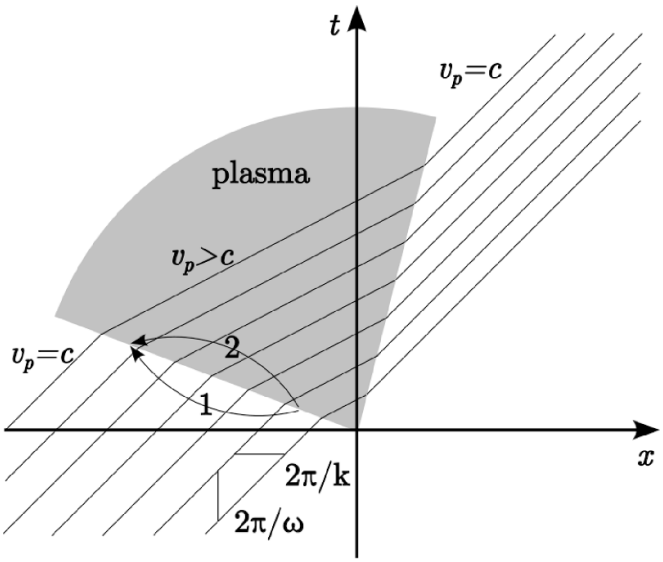

Figure 1. Spacetime diagram of plasma creation and laser frequency upshift. The phase differences are identical for both path 1 and path 2.

In a QED cascade, the created pair plasma interacts with the laser in a manner similar to an ionization front but in a counterpropagating geometry. The refractive index changes in both space and time, and leads to changes in both laser frequency and wavelength. In the following, we will first pictorially explain the change of laser spectrum using a spacetime diagram and then analytically derive the amount of upshift due to the transient and inhomogeneous pair plasma.

4.1. Diagram explanation of laser frequency upshift

Laser propagation can be illustrated using the spacetime diagram, as shown in figure 1. The shaded area in figure 1 represents the pair plasma which grows in time and expands in space. The parallel lines represent the laser wavefront propagating in the x-direction. The vertical and horizontal spacing of the lines correspond to the laser frequency and wavevector, respectively. As the laser propagates through the vacuum-plasma interface, its phase velocity changes from c to $v_p = c/\sqrt{1-\omega_p^2/\omega^2} > c$. The phase of the laser is nevertheless continuous across the interface, represented as non-broken lines in figure 1.

The change of laser frequency and wavenumber results from both the change of phase velocity, denoted as the slope change of the parallel lines in figure 1, and the angle of interface. The interface can be categorized into the following types depending on its angle:

(a) A spatial interface of media is represented by a vertical boundary parallel to the t-axis in the spacetime diagram. When crossing the spatial interface, the laser wavefront conserves its vertical spacing, i.e. its frequency, but its horizontal spacing changes correspondingly, indicating a change in wavenumber.
(b) A temporal interface of media is represented by a horizontal boundary parallel to the x-axis in the spacetime diagram. Across it, the laser wavefront conserves its horizontal spacing but changes its vertical spacing, indicating a change in frequency.
(c) More generally, if the interface involves both spatial and temporal changes of refractive index, the boundary is not parallel to either t- or x-axis, and the laser wavefront spacing changes in both directions, indicating changes in both frequency and wavevector.

Since the laser phase is continuous, any separation on the interface has identical optical paths in both media, leading to the identity

$$k_1\Delta x - \omega_1\Delta t = k_2\Delta x - \omega_2\Delta t, \tag{2}$$

where ω_i and k_i are the frequency and wavevector in the ith medium, and Δt and Δx are arbitrary spacetime distances on the interface. The slope of interface is most conveniently described by the parameter $1/\beta = c\Delta t/\Delta x$. The parameter βc can also be interpreted as the velocity of the interface. Then using the relation $v_{p,i} = \omega_i/k_i$, we can obtain

$$\begin{aligned} \omega_2 &= \left(\frac{\beta^{-1} - c/v_{p1}}{\beta^{-1} - c/v_{p2}}\right)\omega_1, \\ k_2 &= \left(\frac{v_{p1}/c - \beta}{v_{p2}/c - \beta}\right)k_1. \end{aligned} \tag{3}$$

These relations describe how the frequency and wavevector change when the laser propagates through a spacetime interface moving at velocity $v = c\beta$. The shifts of frequency and wavevector can then be expressed as

$$\begin{aligned} \Delta\omega &= \left(\frac{c/v_{p2} - c/v_{p1}}{\beta^{-1} - c/v_{p2}}\right)\omega_1, \\ \Delta k &= \left(\frac{v_{p1}/c - v_{p2}/c}{v_{p2}/c - \beta}\right)k_1. \end{aligned} \tag{4}$$

The process of interface crossing can take place either when the laser propagates faster than the interface ($v_{p1,2} > \beta c$) or when the interface overtakes the laser ($\beta c > v_{p1,2}$). However, the parameter regime $v_{pi} > \beta c > v_{pj}$ ($i \neq j$) forbids laser propagation after it crosses the interface, and hence is nonphysical.

The amount of frequency shift ($\Delta\omega$) and wavevector shift (Δk) with varying interface velocity β is plotted in figure 2 assuming, respectively, (a) $v_{p2} > v_{p1}$ and (b) $v_{p2} < v_{p1}$. Depending on the relation between the interface and laser velocities, the plot can be divided into four regimes, among which the shaded areas are nonphysical.

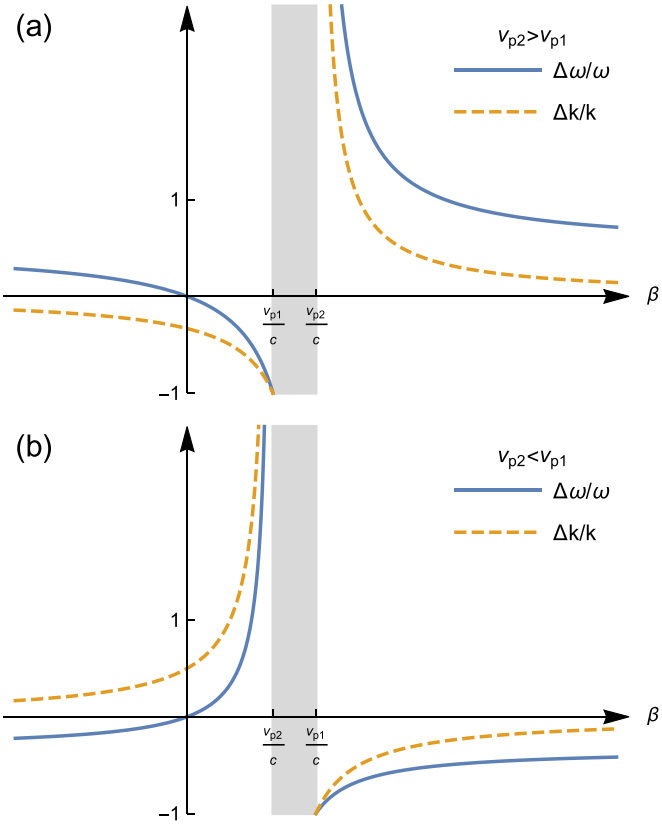

Figure 2. Frequency change ($\Delta\omega$, solid blue curves) and wavevector change (Δk, dashed orange curves) for different interface velocities β assuming (a) $v_{p2} > v_{p1}$ and (b) $v_{p2} < v_{p1}$. The shaded region is nonphysical because the laser cannot propagate in the second medium after crossing the interface.

A subluminal copropagating interface $v_{p1,2} > \beta c \geqslant 0$ traverses through the laser pulse from the laser front to the laser tail. If $v_{p2} > v_{p1}$, the laser wavefront propagates faster after crossing the interface, leading to an increase in wavelength and period. Thus, both the laser frequency and wavevector are downshifted. In the limit of $\beta \to 0$, it reduces to a stationary interface, which downshifts the laser wavevector by v_{p1}/v_{p2} but conserves the laser frequency. As the interface velocity increases, the slower relative motion between the laser wavefront and the interface lengthens the wavefront spreading process, thereby amplifying the downshifts.

A superluminal copropagating interface $\beta c > v_{p1,2} > 0$ traverses through the laser pulse from the laser tail to the front. For $v_{p2} > v_{p1}$, the faster phase velocity in the tail compresses the laser wavefront. This leads to a decrease in wavelength and period, and hence an upshift of laser frequency and wavevector. Similar to the subluminal interface, a smaller relative interface-to-laser velocity lengthens the time of wavefront compression. Thus, the frequency and wavevector upshifts become greater as $\beta c \to v_{p2}$. In the case of a laser crossing a sudden and homogeneous interface $\beta \to \infty$, the spatial separation of the laser wavefront, or wavelength λ, does not change, i.e. $\Delta k = 0$, but the temporal separation is reduced from λ/v_{p1} to λ/v_{p2} so that the frequency is upshifted by a factor v_{p2}/v_{p1}.

A counterpropagating interface $\beta < 0$ traverses through the laser pulse from the laser front to tail. Similar to the scenario of a subluminal copropagating interface, the laser wavefront, which has a faster phase velocity at the front, is lengthened. This causes a downshift of wavevector, $\Delta k < 0$. From the time point of view, the laser wavefronts in the counterpropagating configuration cross the interface at a rate higher than the laser frequency. This allows the laser tail to propagate more time at v_{p2} ($>v_{p1}$) than the front for the same distance, similar to the effect of a superluminal copropagating interface. Thus, the laser wavefront is compressed in time, and the laser frequency is upshifted.

In an electron-beam driven QED cascade, the laser pulse crosses the vacuum-plasma interface twice, including entering and exiting the plasma. The first encounter occurs when the laser pulse and electron beam begin to collide. The pairs are initially created inside the electron beam and thus the vacuum plasma interface has the same Lorentz factor as the beam, i.e. $\beta_1 \approx -1$. (The β factor could locally exceed the unit value since the pair density spacetime gradient is determined by both the particle density and laser intensity. However, the asymptotic speed of the pair plasma front is equal to that of the electron beam.) If we assume a homogeneous plasma, the laser phase velocity changes from c to $v_p = c\Big/\sqrt{1-\omega_p^2/\omega^2} > c$ after crossing the interface. According to (3), the laser frequency and wavevector change to $\omega_2 = 2\omega/(1+c/v_p)$ and $k_2 = 2k/(1+v_p/c)$, respectively. The created pairs lose most of their energy and are subject to the ponderomotive potential of the strong laser pulse. As explained in the last section, the pairs are mostly stopped and partially reflected while expanding in transverse directions. Also, because the fast moving pairs have high energy and contribute very little to the plasma frequency, we can describe the second plasma-vacuum interface with $\beta \sim 0$. Thus, the laser frequency does not change and the wavevector changes as $k_f = k_2(v_p/c)$. Therefore, the vacuum-plasma-vacuum interfaces change the laser frequency and wavevector as

$$\begin{aligned} \omega_f &= \left(\frac{2}{1+c/v_p}\right)\omega \approx \omega + \frac{\omega_p^2}{4\omega}, \\ k_f &= \left(\frac{2}{1+c/v_p}\right)k \approx k + \frac{c\omega_p^2}{4\omega}. \end{aligned} \tag{5}$$

Equation (5) shows that the amount of laser frequency upshift is $\omega_p^2/(4\omega)$. This is lower than the laser frequency upshift in sudden 'flash' ionization by a factor of 2 caused by the finite velocity of the interface. The laser frequency change can be measurable if the pair plasma density needs to reach a non-negligible fraction of the laser frequency. Assuming laser amplitude $a_0 \sim 100$, the pair density needs to reach 10^{21} cm^{-3}.

4.2. Chirp of laser spectrum caused by QED cascade

The above analysis assumes a homogeneous plasma to obtain equation (5). However, the combined processes of pair creation and volume expansion cause the plasma density to be inhomogeneous in both space and time. We illustrate the interaction of the laser and pair plasma in figure 3. The diagram shows that as the laser pulse enters and exits the plasma-vacuum interface, each part of the laser pulse propagates through the plasma at different velocities. Since only the laser center propagates through the densest part of the plasma, it experiences the largest frequency and wavevector upshifts. Therefore, the laser pulse is chirped.

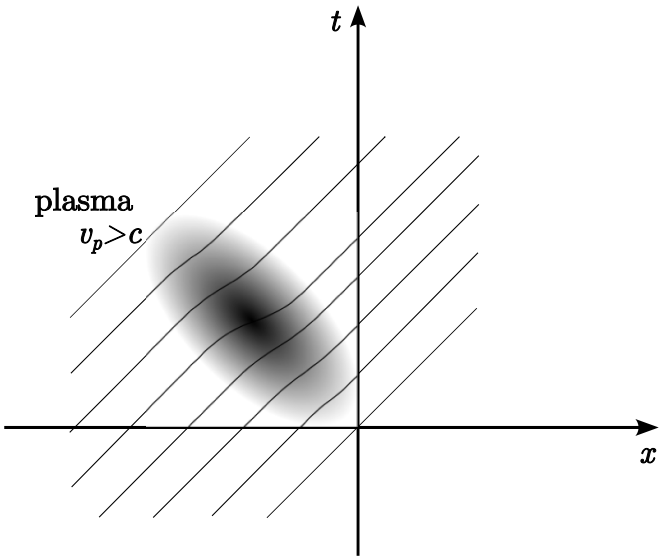

Figure 3. Spacetime diagram of plasma creation and laser frequency upshift.

The chirp profile can be found by tracing the amount of phase shift when the laser propagates through the inhomogeneous plasma. Since the phase shift is different for each part of the laser pulse, it is convenient to define $\xi = x - ct$ denoting the relative delay from the laser front and $\tau = t$ denoting the propagation time. The laser phase can then be written as $\phi = \omega(t - x/v_p) = -\omega\xi/v_p + \omega(1 - c/v_p)\tau$. The expression in the (ξ, τ) coordinate separates the laser phase into its internal phase variation and the induced changes along τ. For a laser propagating in vacuum, $\phi = -\omega\xi/c$ is a constant along τ. If the laser propagates through the plasma as shown in figure 3, the collective plasma effect causes a phase shift $\mathrm{d}\phi = (1 - c/v_p)\mathrm{d}\tau$, which accumulates in τ. For small plasma frequencies, $1 - c/v_p \approx \omega_p^2/(2\omega)$. Each part of the laser at ξ propagates through the plasma at $(\xi + c\tau', \tau')$ over the range $-\infty < \tau' < \tau$. Thus, the total phase shift can be found as

$$\Delta\phi = \int_{-\infty}^{\tau} \omega_p^2(\xi + \tau', \tau')/(2\omega)\mathrm{d}\tau'. \tag{6}$$

Neglecting the small change of $1/\omega$ and transforming back to the (x, t) coordinate, we have

$$\Delta\phi = \frac{1}{2\omega}\int_{-\infty}^{t} \omega_p^2(x - ct + ct', t')\mathrm{d}t'. \tag{7}$$

The frequency and wavevector after propagating through inhomogeneous plasma can thus be expressed as

$$\Delta\omega(x,t) = \frac{\partial\Delta\phi}{\partial t} = \frac{\omega_p^2(x,t)}{2\omega} + \frac{1}{2\omega}\int_{-\infty}^{t}[\partial_t\omega_p^2(x-ct+ct',t')]\mathrm{d}t', \tag{8}$$

$$\Delta k(x,t) = -\frac{\partial\Delta\phi}{\partial x} = -\frac{1}{2\omega}\int_{-\infty}^{t}[\partial_x\omega_p^2(x-ct+ct',t')]\mathrm{d}t'. \tag{9}$$

Note that $\partial_t\omega_p^2 = -c\partial_x\omega_p^2$, so the dispersion relation $\Delta\omega - c\Delta k = \omega_p^2/(2\omega)$ is automatically satisfied. We can further simplify the expressions by noting that $\omega_p^2(x,t) = \int_{-\infty}^{t}[\partial_{t'}\omega_p^2(x-ct+ct',t')]\mathrm{d}t'$ and $(\partial_t+\partial_{t'})\omega_p^2(x-ct+ct',t') = [\partial_T\omega_p^2(X,T)]_{X=x-ct+ct'}^{T=t'}$, then we obtain the expressions reported in [6, 7]

$$\Delta\omega(x,t) = \frac{1}{2\omega}\int_{-\infty}^{t}[\partial_T\omega_p^2(X,T)]_{X=x-ct+ct'}^{T=t'}\mathrm{d}t', \tag{10}$$

$$\Delta k(x,t) = -\frac{1}{2\omega}\int_{-\infty}^{t}[\partial_X\omega_p^2(X,T)]_{X=x-ct+ct'}^{T=t'}\mathrm{d}t'. \tag{11}$$

The expressions show a very intuitive picture: the change of laser frequency and wavevector are caused by the integration of temporal and spatial change of plasma frequency calculated at the retarded position $X = x - c(t-t')$. If the plasma moves with velocity $-c$, then $\partial_T\omega_p^2(X,T) = -c\partial_X\omega_p^2(X,T)$ and hence the amount of frequency and wavevector upshift only differ by a factor of c.

Because the laser chirp is related to the rapidity of the plasma frequency change $\partial_T\omega_p^2(X,T)$, the signal could be much larger than the laser frequency shift for small plasma size. In the aforementioned QED cascade, the laser pulse has a typical duration of 100 fs corresponding to 30 μm in length, but the plasma only has <10 μm length. Thus, the instantaneous laser frequency upshift could be several times higher than the central frequency change of the whole pulse. In other words, the pair plasma is created when a small electron beam encounters the most intense region of the laser pulse and hence only induces a laser frequency upshift near its intensity peak. When averaging over the whole laser pulse, the frequency upshift decreases by a large factor.

5. Conclusion

The QED plasma dynamics are distinguished from traditional electron-ion plasmas by a number of physical aspects, including special relativistic effects, radiation-reaction effects, and high mobility under laser pressure. Exploiting the laser frequency upshift relaxes the conditions for QED plasma detection. Thus, creating an observable pair plasma through strong-field QED cascades in terrestrial laboratories becomes possible with state-of-the-art technologies.

Adopting the electron-beam-laser collision approach, the minimum parameters for testing QED plasma phenomena include laser intensity of 10^{23} W cm^{-2} and electron beam energy density of 10^{18} J m^{-3} ($\gamma n_0 \sim 10^{25}$ cm^{-3}). The required energy density can be readily produced by a conventional electron beam accelerator. Its production at a strong laser facility might also become possible if the LWFA technique can overcome the trade-off between high beam energy and high total electron charge. If the high energy-density electron beam is colocated with a PW-class laser, the collision creates QED pairs with growing density and decreasing energy. In contrast to the direct all-optical laser-laser collision approach, the electron-beam driven QED cascade converts high energy beams into pairs with low energy and high density, both of which contribute to higher plasma frequency. The use of a high energy electron beam reduces the required laser intensity. The lower laser intensity means that the produced pairs are less energetic, making the plasma frequency larger for the same pair density.

Identifying the conditions for creating observable QED plasma is timely in view of the present planning of QED facilities. With current technology, the highest quantum nonlinearity parameter χ is achieved using conventional electron accelerators. The undergoing Stanford E-320 experiment [20] uses a 10 GeV beam and a 10^{20} W cm^{-2} laser to achieve $\chi \sim 1$. The electron beam energy density, assuming that the 2 nC beam can be compressed to 0.5 μm $\times$ (3 μm)^2 size, could reach $\gamma_0 n_0 \sim 10^{25}$ cm^{-3}. Creating an observable QED plasma requires an upgrade of the laser by two order of magnitude, reaching $\chi \sim 100$. The LUXE experiment at DESY proposes [73] using a 17.5 GeV beam and 10^{20}–10^{21} W cm^{-2} to achieve $\chi \sim 1$–3. The beam at the highest energy configuration is limited to 0.25 nC charge and ~50 fs length, hence it needs significant focusing to exhibit collective plasma effects.

Data availability statement

No new data were created or analysed in this study.

Acknowledgment

This work was supported by DOE Grants DE-NA0003871, NNSA DE-SC0021248, and DE-AC02-76SF00515.

ORCID iDs

Kenan Qu https://orcid.org/0000-0002-6186-1985
Sebastian Meuren https://orcid.org/0000-0002-2744-7756
Nathaniel J Fisch https://orcid.org/0000-0002-0301-7380

References

[1] Schwinger J 1951 *Phys. Rev.* **82** 664
[2] Uzdensky D A and Rightley S 2014 *Rep. Prog. Phys.* **77** 036902

[3] Grismayer T, Vranic M, Martins J L, Fonseca R A and Silva L O 2016 *Phys. Plasmas* **23** 056706
[4] Uzdensky D *et al* 2019 Extreme plasma astrophysics (arXiv:1903.05328)
[5] Zhang P, Bulanov S S, Seipt D, Arefiev A V and Thomas A G R 2020 *Phys. Plasmas* **27** 050601
[6] Qu K, Meuren S and Fisch N J 2021 *Phys. Rev. Lett.* **127** 095001
[7] Qu K, Meuren S and Fisch N J 2022 *Phys. Plasmas* **29** 042117
[8] Ruffini R, Vereshchagin G and Xue S S 2010 *Phys. Rep.* **487** 1–140
[9] Kaspi V M and Beloborodov A M 2017 *Annu. Rev. Astron. Astrophys.* **55** 261
[10] Cerutti B and Beloborodov A M 2017 *Space Sci. Rev.* **207** 111
[11] Zhang B 2020 *Nature* **587** 45–53
[12] Cartlidge E 2018 *Science* **359** 382
[13] Bromage J *et al* 2019 *High Power Laser Sci. Eng.* **7** e4
[14] Danson C N *et al* 2019 *High Power Laser Sci. Eng.* **7** e54
[15] Yoon J W, Jeon C, Shin J, Lee S K, Lee H W, Choi I W, Kim H T, Sung J H and Nam C H 2019 *Opt. Express* **27** 20412–20
[16] Bula C *et al* 1996 *Phys. Rev. Lett.* **76** 3116
[17] Burke D L *et al* 1997 *Phys. Rev. Lett.* **79** 1626
[18] Cole J M *et al* 2018 *Phys. Rev.* X **8** 011020
[19] Poder K *et al* 2018 *Phys. Rev.* X **8** 031004
[20] Meuren S 2022 Light-matter interactions at extreme intensities and densities: reaching the Schwinger limit *APS April Meeting Abstracts* (*APS Meeting Abstracts* vol 2022) p H07.003 (available at: https://meetings.aps.org/Meeting/APR22/Session/H07.3)
[21] SLAC Site Office 2016 *Technical Design Report for the FACET-II Project at SLAC National Accelerator Laboratory* SLAC-R-1072 (available at: www.slac.stanford.edu/pubs/slacreports/reports19/slac-r-1072.pdf)
[22] Meuren S, Bucksbaum P H, Fisch N J, Fiúza F, Glenzer S, Hogan M J, Qu K, Reis D A, White G and Yakimenko V 2020 On seminal HEDP research opportunities enabled by colocating multi-petawatt laser with high-density electron beams (arXiv:2002.10051)
[23] Di Piazza A, Müller C, Hatsagortsyan K Z and Keitel C H 2012 *Rev. Mod. Phys.* **84** 1177
[24] Sokolov I V, Naumova N M, Nees J A and Mourou G A 2010 *Phys. Rev. Lett.* **105** 195005
[25] Hu H, Müller C and Keitel C H 2010 *Phys. Rev. Lett.* **105** 080401
[26] Thomas A G R, Ridgers C P, Bulanov S S, Griffin B J and Mangles S P D 2012 *Phys. Rev.* X **2** 041004
[27] Neitz N and Di Piazza A 2013 *Phys. Rev. Lett.* **111** 054802
[28] Bulanov S S, Schroeder C B, Esarey E and Leemans W P 2013 *Phys. Rev.* A **87** 062110
[29] Blackburn T G, Ridgers C P, Kirk J G and Bell A R 2014 *Phys. Rev. Lett.* **112** 015001
[30] Green D G and Harvey C N 2014 *Phys. Rev. Lett.* **112** 164801
[31] Vranic M, Martins J L, Vieira J, Fonseca R A and Silva L O 2014 *Phys. Rev. Lett.* **113** 134801
[32] Blackburn T G, Ilderton A, Murphy C D and Marklund M 2017 *Phys. Rev.* A **96** 022128
[33] Vranic M, Klimo O, Korn G and Weber S 2018 *Sci. Rep.* **8** 4702
[34] Magnusson J, Gonoskov A, Marklund M, Esirkepov T Z, Koga J K, Kondo K, Kando M, Bulanov S V, Korn G and Bulanov S S 2019 *Phys. Rev. Lett.* **122** 254801
[35] Morgenthaler F R 1958 *IEEE Trans. Microw. Theory Tech.* **6** 167
[36] Wilks S C, Dawson J M and Mori W B 1988 *Phys. Rev. Lett.* **61** 337
[37] Esarey E, Ting A and Sprangle P 1990 *Phys. Rev.* A **42** 3526
[38] Wood W M, Siders C W and Downer M C 1991 *Phys. Rev. Lett.* **67** 3523
[39] Mendonça J T 2000 *Theory of Photon Acceleration* (London: Institute of Physics Publishing) (available at: http://www.physics.gov.az/book_T/Mendonca.pdf)
[40] Mendonça J T and Shukla P K 2002 *Phys. Scr.* **65** 160
[41] Qu K and Fisch N J 2019 *Phys. Plasmas* **26** 083105
[42] Shcherbakov M R, Werner K, Fan Z, Talisa N, Chowdhury E and Shvets G 2019 *Nat. Commun.* **10** 1345
[43] Nishida A, Yugami N, Higashiguchi T, Otsuka T, Suzuki F, Nakata M, Sentoku Y and Kodama R 2012 *Appl. Phys. Lett.* **101** 161118
[44] Qu K, Jia Q, Edwards M R and Fisch N J 2018 *Phys. Rev.* E **98** 023202
[45] Edwards M R, Qu K, Jia Q, Mikhailova J M and Fisch N J 2018 *Phys. Plasmas* **25** 053102
[46] Bulanov S S, Fedotov A M and Pegoraro F 2005 *Phys. Rev.* E **71** 016404
[47] Peng H, Riconda C, Weber S, Zhou C T and Ruan S C 2021 *Phys. Rev. Appl.* **15** 054053
[48] Jirka M, Klimo O, Bulanov S V, Esirkepov T Z, Gelfer E, Bulanov S S, Weber S and Korn G 2016 *Phys. Rev.* E **93** 023207
[49] Grismayer T, Vranic M, Martins J L, Fonseca R A and Silva L O 2017 *Phys. Rev.* E **95** 023210
[50] Griffith A, Qu K and Fisch N J 2022 *Phys. Plasmas* **29** 073104
[51] Gonsalves A J *et al* 2019 *Phys. Rev. Lett.* **122** 084801
[52] Andreev N E, Kuznetsov S V, Pogosova A A, Steinhauer L C and Kimura W D 2003 *Phys. Rev. ST Accel. Beams* **6** 041301
[53] Welch J R, Zgadzaj R, Polyanskiy M, Zhang C, Pogorelsky I and Downer M C 2017 Mid-IR, CO_2-laser driven, self-modulated wakes *Conf. on Lasers and Electro-Optics* (Optica Publishing Group) p FM2D.6
[54] Kumar P, Yu K, Zgadzaj R, Downer M, Petrushina I, Samulyak R, Litvinenko V and Vafaei-Najafabadi N 2021 *Phys. Plasmas* **28** 013102
[55] Brunetti E, Campbell R N, Lovell J and Jaroszynski D A 2022 *Sci. Rep.* **12** 6703
[56] Felsen L and Whitman G 1970 *IEEE Trans. Antennas Propag.* **18** 242–53
[57] Kravtsov Y A, Ostrovsky L A and Stepanov N S 1974 *Proc. IEEE* **62** 1492–510
[58] AuYeung J C 1983 *Opt. Lett.* **8** 148–50
[59] Stepanov N S 1993 *Radiophys. Quantum Electron.* **36** 401–9
[60] Ostrovskii L A and Stepanov N S 1971 *Radiophys. Quantum Electron.* **14** 387–419
[61] Jiang C L 1975 *IEEE Trans. Antennas Propag.* **23** 83–90
[62] Lampe M, Ott E and Walker J H 1978 *Phys. Fluids* **21** 42–54
[63] Wilks S C, Dawson J M, Mori W B, Katsouleas T and Jones M E 1989 *Phys. Rev. Lett.* **62** 2600
[64] Mori W 1991 *Phys. Rev.* A **44** 5118
[65] Kalluri D and Goteti V 1992 *J. Appl. Phys.* **72** 4575–80
[66] Savage R, Brogle R, Mori W and Joshi C 1993 *IEEE Trans. Plasma Sci.* **21** 5–19
[67] Yablonovitch E 1973 *Phys. Rev. Lett.* **31** 877
[68] Joshi C J, Clayton C, Marsh K, Hopkins D, Sessler A and Whittum D 1990 *IEEE Trans. Plasma Sci.* **18** 814–8
[69] Kuo S P 1990 *Phys. Rev. Lett.* **65** 1000
[70] Yugami N, Niiyama T, Higashiguchi T, Gao H, Sasaki S, Ito H and Nishida Y 2002 *Phys. Rev.* E **65** 036505
[71] Geltner I, Avitzour Y and Suckewer S 2002 *Appl. Phys. Lett.* **81** 226
[72] Avitzour Y, Geltner I and Suckewer S 2005 *J. Phys.* B **38** 779
[73] Abramowicz H *et al* 2019 Letter of intent for the LUXE experiment (arXiv:1909.00860)